

# Wheel-Ground Interaction Modelling and Torque Distribution for a Redundant Mobile Robot

Yuan Ping Li\*, Teresa Zielinska†, Marcelo H. Ang Jr.\* and Wei Lin‡

\*Department of Mechanical Engineering  
National University of Singapore, Singapore  
Email: {liyuanping,mpeangh}@nus.edu.sg

†Faculty of Power and Aeronautical Engineering  
Warsaw University of Technology, Poland  
Email: teresaz@meil.pw.edu.pl

‡Singapore Institute of Manufacturing Technology, Singapore  
Email: wlin@SIMTech.a-star.edu.sg

**Abstract**—An operational space dynamic model of a redundantly actuated wheeled mobile robot taking into account the wheel-ground interaction is derived based on vehicle dynamics. The conditions for the robot to avoid slip are derived for both torque and motion. Two torque distribution schemes based on different criteria are proposed. The non-slip condition for motion is utilized to plan slip avoidance paths. The null space joint torques are utilized to fulfill the non-slip condition for torque and avoid actuator torque limits violation. Simulations results are presented to demonstrate the effects of wheel-ground interaction and performance of the proposed torque distribution schemes.

## I. INTRODUCTION

An omnidirectional mobile robot (Fig. 1) with four Powered Caster Wheels (PCW) was developed. The robot is characterized by its omnidirectional mobility, high payload (200 kg) and actuation redundancy.



Fig. 1. Omnidirectional mobile robot with 4 powered caster wheels.

Kinematic and dynamic modelling of this kind of robots are well studied in the literature [1]–[5]. However, these literature implicitly assume single point contact between the wheel and ground. Under this assumption, the kinematic and dynamic models were derived based on the pure rolling without slipping condition. Such an condition may not be true in real situations and experimental results have shown that wheel motion may suffer significant slip using control algorithms based on the

simplified models [6], [7]. This is due to the fact that the condition for the wheel to satisfy the pure rolling without slipping constraint are seldom studied in the literature. The actual wheel-ground interaction needs to be considered in order to improve the robot motion control.

The topic of wheel-ground interaction is under the investigations of “Vehicle Dynamics” [8], [9]. For the purpose of practical use, simplified vehicle dynamic models are applied to model the wheel-ground interaction in this paper. Based on vehicle dynamics, explicit conditions for the wheel to satisfy the pure rolling without slipping constraint are derived for both motion and torque. The actuation redundancy of the robot is then resolved to fulfill the non-slip conditions. The contributions of this paper are, firstly, the derivation of a more realistic dynamic model and non-slip conditions based on vehicle dynamics; secondly, the derivation of the dynamically consistent generalized inverse for a redundant mobile robot with passive joints; lastly, the utilization of actuation redundancy of the robot for torque distribution problem.

This paper is organized as follows. Sec. II presents the kinematic and dynamic modelling of the robot under the pure rolling without slipping constraint. Sec. III models the wheel-ground interaction based on vehicle dynamics and derives the non-slip conditions. Two torque distribution schemes are proposed in Sec. IV followed by the simulation results in Sec. V. The paper is concluded in Sec. VI.

## II. MOTION SYNTHESIS WITHOUT WHEEL-GROUND INTERACTION

### A. Kinematic Modelling

The mobile robot shown in Fig. 1 consists of 4 PCWs, each actuated by two motors: one for rolling and the other for steering. Fig. 2 shows the frame assignments and parameter definitions of the overall mobile robot.

A powered caster wheel is modelled as a 3-DOF serial manipulator and only the rolling  $\rho$  and steering  $\phi$  joints are actuated while the twisting joint  $\sigma$  is passive [10]. The

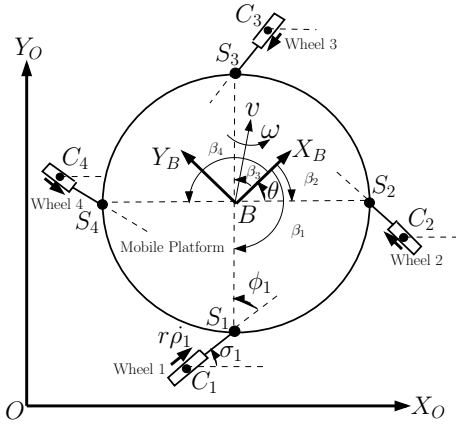


Fig. 2. Frame assignments, parameter and variable definitions of the mobile robot shown in Fig. 1.

differential kinematics of one wheel module is given as:

$$\dot{x} = J_i \cdot \dot{q}_i \quad (1)$$

where  $\dot{x} = [v, \omega]^T \in R^{3 \times 1}$  describes the motion of the base w.r.t. the base frame  $\mathbf{B}$ ;  $\dot{q}_i = [\dot{\sigma}_i, \dot{\rho}_i, \dot{\phi}_i]^T$  describes the wheel's joint motion and  $J_i$ , the jacobian for wheel  $i$  ( $i = 1, \dots, 4$ ) is given as:

$$J_i = \begin{bmatrix} hS_{\beta_i} + bS_{\beta_i - \phi_i} & rC_{\beta_i - \phi_i} & hS_{\beta_i} \\ hC_{\beta_i} & bC_{\beta_i - \phi_i} & rS_{\beta_i - \phi_i} \\ 1 & 0 & 1 \end{bmatrix} \quad (2)$$

where  $r$  and  $b$  are caster wheel radius and offset;  $h$  and  $\beta_i$  are location parameters for wheel  $i$  w.r.t. the base frame  $\mathbf{B}$ ;  $\phi_i$  is the steering angle;  $S_*$  and  $C_*$  denote  $\sin(\cdot)$  and  $\cos(\cdot)$  for scalar respectively.

It is easy to verify that the determinant of matrix  $J_i$  is  $br$  which implies that  $J_i$  is always invertible.

It is shown in [11] that the differential kinematics of the overall robot is given as:

$$A\dot{x} = B\dot{q} \quad (3)$$

where  $A \in R^{8 \times 3}$  and  $B \in R^{8 \times 8}$  are the forward and inverse kinematic matrices of the robot respectively;  $\dot{q} \in R^{8 \times 1}$  describes the motion of all the joints of the robot; It is shown in [11] that  $A^+$  (pseudoinverse of matrix  $\mathbf{A}$ ) always exists and matrix  $\mathbf{B}$  is always invertible. For convenience, we define  $J_I = B^{-1}A$  as the inverse jacobian and  $J_F = A^+B$  as the forward jacobian of the robot. Note that  $[\cdot]^+$  in this paper denotes the pseudoinverse of quantity  $[\cdot]$ .

### B. Dynamic Modelling

The dynamic model of each PCW module using *Operational Space Formulation* [12] is derived as:

$$F_i = \Lambda_i(x)\ddot{x} + \mu_i(x, \dot{x}) + \eta_i(x) \quad (4)$$

where  $F_i$ ,  $\Lambda_i$ ,  $\mu_i$  and  $\eta_i$  are resultant force vector, kinetic energy matrix, Coriolis/centrifugal force vector and gravity force vector for wheel  $i$  ( $i = 1, \dots, 4$ ) in operational space respectively.

The mobile robot can be considered as 4 cooperative manipulators (PCWs) grasping a common object at the end-effectors (center of the mobile robot). The *Augmented Object Model* states that the dynamics of the composite system is found by summing the operational space dynamics of the load and each of the robot [13]. So the augmented kinetic energy matrix  $\Lambda^*(x)$ , augmented Coriolis/centrifugal force vector  $\mu^*(x, \dot{x})$  are given as:

$$\Lambda^*(x) = \sum \Lambda_i(x) + \Lambda_l(x) \quad (5)$$

$$\mu^*(x, \dot{x}) = \sum \mu_i(x, \dot{x}) + \mu_l(x, \dot{x}) \quad (6)$$

where  $\Lambda_l(x)$  and  $\mu_l(x, \dot{x})$  are kinetic energy matrix and Coriolis/centrifugal force vector of the load with respect to the operational point. The gravity force is ignored since the mobile robot is assumed to move on horizontal surface.

The dynamic formulation of the augmented system in operational space is then given as:

$$F^* = \Lambda^* \ddot{x} + \mu^* \quad (7)$$

The implementation of above dynamic model in the control of the mobile robot (Fig. 1) is presented in [7], where experimental results show that slip occurs under conventional methods of control. That is expected since the wheel-ground interaction was not considered.

## III. VEHICLE DYNAMICS ANALYSIS

### A. Resistance to Wheel Motion

Assuming the wheel plane remains perpendicular to the ground, the motions of a PCW w.r.t. the ground occur in two directions (Fig. 3):  $\dot{\rho}$ , rotation about the rolling (horizontal) axis  $\hat{y}_C$ ; and  $\dot{\sigma}$ , rotation about the twisting (vertical) axis  $\hat{z}_C$ .  $Q$  is the vertical force that the robot exerts on the ground. Note that the steering motion of a PCW i.e.  $\dot{\phi}$ , is the relative motion between the wheel and the chassis of the mobile platform, thus it is not generated by the wheel-ground interaction.

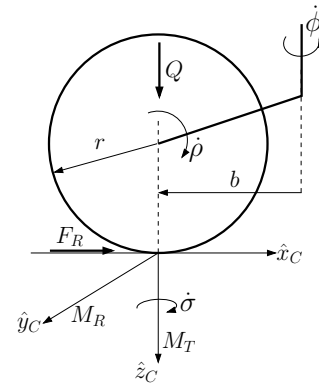


Fig. 3. Motion resistance forces/moments on a powered caster wheel

The rolling motion generates a horizontal reactive force  $F_R$  and a horizontal reactive moment  $M_R$  while the twisting motion generates a pure reactive moment  $M_T$  in the vertical direction. Ignoring the aerodynamic forces and other external

forces and assuming the ground is horizontal and does not deform, the above three quantities are defined in vehicle dynamics literature (e.g. [14]) as:

- Rolling Friction:  $F_R = \text{sgn}(\dot{\rho})f_oQ\hat{x}_C$ ;
- Rolling Resistance:  $M_R = \text{sgn}(\dot{\rho})f_oQr\hat{y}_C$ ;
- Turning Resistance:  $M_T = \text{sgn}(\dot{\sigma})\mu_oQp\hat{z}_C$ .

where  $f_o$  and  $\mu_o$  are the rolling friction coefficient and cohesion coefficient respectively;  $r$  is the wheel radius and  $p$  is the geometrical averaging radius of the contact patch. The signum function in the formulas shows that the frictional forces and moments are acting against the particular joint motions.

In the case of PCW, the rolling resistance  $M_R$  is overcome by the rolling joint torque  $\Gamma_\rho$  and the turning resistance  $M_T$  is overcome by the steering joint torque  $\Gamma_\phi$ .

### B. Dynamics of One Wheel

Without considering the motion resistances and other external forces, the dynamics of a single wheel is given by the Lagrangian formulation:

$$\Gamma_i = I_i(q_i)\ddot{q}_i + P_i(q_i, \dot{q}_i) + G_i(q_i) \quad (8)$$

where  $\Gamma_i = [\Gamma_{\rho_i}, \Gamma_{\phi_i}]^T$  is the actuated joints torque vector;  $I_i$  is the kinetic energy matrix;  $P_i$  is Coriolis/centrifugal force vector and  $G_i$  is the gravity force vector. Subscript  $i$  denotes the wheel number.

Ignoring the gravity term (which is zero in our case) and considering the motion resistances, the dynamics of one wheel is rewritten as:

$$\Gamma_i = I_i(q_i)\ddot{q}_i + P_i(q_i, \dot{q}_i) - M_{res_i} \quad (9)$$

where  $M_{res_i} = [M_{R_i}, M_{T_i}]^T$  is the motion resistance vector.

### C. Dynamics of the Robot

Considering the motion resistances as external forces acting at the operational point, the augmented object dynamic model of the robot (Eq. (7)) is compensated and rewritten as:

$$F^\oplus = \Lambda^* \ddot{x} + \mu^* F_{res} \quad (10)$$

where  $F_{res}$  is the resultant force/moment vector generated by the wheel-ground interaction at operational space. Based on the force/moment analysis for one wheel in Fig. 3,  $F_{res}$  can be derived as:

$$F_{res} = \begin{bmatrix} \sum F_{R_i} \cos(\sigma_i) \\ \sum F_{R_i} \sin(\sigma_i) \\ \sum (M_{T_i} + F_{R_i} p_{C_i}) \end{bmatrix} \quad (11)$$

where  $p_{C_i}$  is the position vector from the center of the robot to the center of the contact patch of wheel  $i$ .

### D. Non-Slip Condition

In order for the robot to move without slipping, joint torques  $\Gamma$  must be smaller than the moment due to static friction  $\mu Q$  ( $\mu$  is the coefficient of static friction). Non-slip condition (necessary but not sufficient) for joint torques of one PCW can then be derived as:

$$\Gamma_i < \begin{bmatrix} \mu Q r \\ \mu Q b \end{bmatrix} \quad (12)$$

Based on Eq. (4) and (8) and ignoring the Coriolis/centrifugal forces, Eq. (12) can be rewritten as:

$$[J_i^T \Lambda_i]_a \ddot{x} < \begin{bmatrix} \mu Q r \\ \mu Q b \end{bmatrix} + M_{res_i} \quad (13)$$

where  $[ ]_a$  is defined as the particular rows of matrix or vector that are corresponding to the actuated joints.

Therefore, non-slip condition (necessary but not sufficient) for robot motion is obtained as:

$$\ddot{x} < [J_i^T \Lambda_i]_a^+ \left( \begin{bmatrix} \mu Q r \\ \mu Q b \end{bmatrix} + M_{res_i} \right) \quad (14)$$

It can be verified that the pseudoinverse of matrix  $[J_i^T \Lambda_i]_a$  always exists since matrices  $J_i$  and  $\Lambda_i$  are always invertible.

## IV. TORQUE DISTRIBUTION BASED ON ACTUATION REDUNDANCY

Two torque distribution schemes based on different criteria are presented in this section which are:

- Minimum Torque Norm (MTN);
- Minimum Internal Force and Dynamical Consistence (MIFDC).

Both torque distribution schemes utilize the null space of the jacobian or its generalized inverse to fulfill the non-slip condition and avoid the joint torque limit violation.

The control diagram of the robot is shown in Fig. 4.

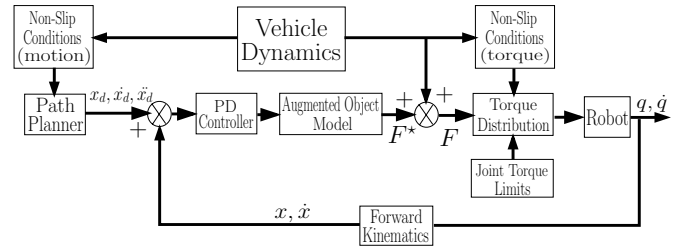


Fig. 4. Control diagram

In the control diagram, the path planner plans desired trajectories that satisfy the non-slip condition for motion Eq. (14). The ‘‘Torque Distribution’’ block in the control diagram can be either of the two torque distribution schemes presented below.

### A. Minimum Torque Norm (MTN)

The dual form of Eq. (3) for force/torque relationship gives:

$$F^\oplus = J_I^T \Gamma \quad (15)$$

Therefore, one general solution of Eq. (15) is given as:

$$\Gamma = (J_I^T)^+ F^\oplus + [E_{8 \times 8} \quad (J_I^T)^+ J_I^T] \Gamma_o \quad (16)$$

where  $E_{8 \times 8}$  is an 8 × 8 identity matrix; and  $\Gamma_o$  is an arbitrary vector.

The first term in the right hand side of Eq. (16) is the torque component that will generate the resultant operational force  $F^\oplus$  while the second term is the torque component in the null space of matrix  $(J_I^T)^+$  that generates no effect on  $F^\oplus$ . The vector  $\Gamma_o$  is set to zero except the case when the non-slip condition Eq. (12) is not satisfied or when the joint torque limit is exceeded. The case when  $\Gamma_o = O$  provides the solution that minimizes the joint torque norm  $\|\Gamma\|$  [15].

### B. Minimum Internal Force and Dynamical Consistence (MIFDC)

The force/torque relationship in general solution form is given as:

$$\Gamma = J_F^T F^\oplus + (E_{8 \times 8} \quad J_F^T \bar{J}_F^T) \Gamma_o \quad (17)$$

where  $\bar{J}_F^T$  is an arbitrary generalized inverse of matrix  $J_F^T$ . Vector  $\Gamma_o$  is chosen in the same way as the MTN scheme. So in the cases when both slip and torque limit violation are avoided,  $\Gamma_o$  is set to be zero and the solution of Eq. (17) becomes:

$$\Gamma = J_F^T F^\oplus \quad (18)$$

It is shown in [7] that by using  $J_F = B^T A^{+T}$ , the differences between every pair of contact forces projected on the line that connects that pair of contact points are minimized. This minimizes the internal forces generated on the chassis of the robot. In the case when Eq. (18) provides the exact solution for Eq. (15), there is no internal force generated on the body, i.e. the ‘‘rigidity’’ of the robot is maintained. However, the operational force that used in [7] didn’t consider the effects of ground-wheel interaction. Therefore, by replacing the operational force  $F^\oplus$  in Eq. (7) with the force in Eq. (10), Eq. (18) will provide a solution that minimizes the internal forces generated on the robot body in a more realistic sense. This is expected because by taking the ground-wheel interaction into account, the more accurate resultant force in operational space is modelled.

Below we will derive a unique generalized inverse  $\bar{J}_F^T$  which is consistent with the system dynamics.

For wheel  $i$ , the relationship between the joint space Eq. (8) and operational space Eq. (4) dynamic model is expressed as:

$$M_i(q_i) \ddot{q}_i + P_i(q_i, \dot{q}_i) + G_i(q_i) = J_i^T [\Lambda_i(x) \ddot{x} + \mu_i(x, \dot{x}) + \eta_i(x)] \quad (19)$$

This is the extension of force/torque duality in dynamic case [12].

Ignoring the gravity term, we can construct the actuated joints torque vector  $\Gamma$  from Eq. (19) as:

$$\Gamma = \begin{bmatrix} [J_1^T \Lambda_1]_a \\ [J_2^T \Lambda_2]_a \\ [J_3^T \Lambda_3]_a \\ [J_4^T \Lambda_4]_a \end{bmatrix} \ddot{x} + \begin{bmatrix} [J_1^T \mu_1]_a \\ [J_2^T \mu_2]_a \\ [J_3^T \mu_3]_a \\ [J_4^T \mu_4]_a \end{bmatrix} \quad (20)$$

With the definition  $\Lambda = (JM^{-1}J^T)^{-1}$  [12], Eq. (20) can be rewritten as:

$$\Gamma = \begin{bmatrix} [J_1^T (J_1 M_1^{-1} J_1^T)^{-1}]_a \\ [J_2^T (J_2 M_2^{-1} J_2^T)^{-1}]_a \\ [J_3^T (J_3 M_3^{-1} J_3^T)^{-1}]_a \\ [J_4^T (J_4 M_4^{-1} J_4^T)^{-1}]_a \end{bmatrix} \ddot{x} + P_a \quad (21)$$

where  $P_a$  is the second term in the right hand side of Eq. (20).

Due to the fact that  $J_i$  is always invertible and so is  $M_i$ , Eq. (21) can be simplified as:

$$\Gamma = \begin{bmatrix} [M_1 J_1^{-1}]_a \\ [M_2 J_2^{-1}]_a \\ [M_3 J_3^{-1}]_a \\ [M_4 J_4^{-1}]_a \end{bmatrix} \ddot{x} + P_a \quad (22)$$

Eq. (22) can be further simplified as:

$$\Gamma = [M_a \quad M_p] \begin{bmatrix} J_I \\ J_p \end{bmatrix} \ddot{x} + P_a \quad (23)$$

where  $M_a$  is the portion corresponding to the inverse kinematic jacobian  $J_I$  while  $M_p$  and  $J_p$  are the portions corresponding to the passive components.

Next we equating the right hand sides of Eq. (23) and (17):

$$(M_a J_I + M_p J_p) \ddot{x} + P_a = J_F^T F^\oplus + (E_{8 \times 8} \quad J_F^T \bar{J}_F^T) \Gamma_o \quad (24)$$

Due to the invertibility of  $J_i$  and  $M_i$ ,  $(M_a J_I)^+$  always exists. Pre-multiplying both sides of Eq. (24) by  $(M_a J_I)^+$ , we obtain an equation that expresses the relationship between  $\ddot{x}$  and  $F^\oplus$ :

$$[E_{3 \times 3} + (M_a J_I)^+ M_p J_p] \ddot{x} + (M_a J_I)^+ P_a = (M_a J_I)^+ J_F^T F^\oplus + (M_a J_I)^+ (E_{8 \times 8} \quad J_F^T \bar{J}_F^T) \Gamma_o \quad (25)$$

It can be verified that  $[E_{3 \times 3} + (M_a J_I)^+ M_p J_p]$  is not singular since it is equivalent to the kinetic energy matrix quantity. Thus, in order for the joint torques associated with the null space in Eq. (25) not to produce any operational acceleration, it is necessary that

$$(M_a J_I)^+ (E_{8 \times 8} \quad J_F^T \bar{J}_F^T) \Gamma_o = 0 \quad (26)$$

Substituting  $(M_a J_I)^+ = (J_I^T M_a^T M_a J_I)^{-1} J_I^T M_a^T$  into Eq. (26), Eq. (26) is equivalent to:

$$J_I^T M_a^T (E_{8 \times 8} \quad J_F^T \bar{J}_F^T) \Gamma_o = 0 \quad (27)$$

Therefore, a unique generalized inverse of  $J_F^T$  that is consistent with the system dynamics can be resolved from Eq. (27) as:

$$\bar{J}_F^T = (J_F M_a J_I)^{-T} J_I^T M_a^T \quad (28)$$

By taking the passive joints and wheel-ground interaction into account, our results complement the work of ‘‘Dynamic Consistency in Multi-Arm System’’ [16].

## V. SIMULATION RESULTS

All the simulations presented in this section use the control diagram shown in Fig. 4. Actual parameters of the robot (Fig. 1) shown in Table. I are used in the simulations.

TABLE I  
SIMULATION PARAMETERS

parameters	values	parameters	values
$r$	0.055 (m)	$f_o$	0.06
$b$	0.020 (m)	$\mu_o$	0.4
$h$	0.219 (m)	$\mu$	0.6
$m_r$	0.65 (kg)	$Q$	310.49 (N)
$m_h$	2 (kg)	$a$	0.027 (m)
$m_b$	29 (kg)	$b$	0.021 (m)

In Table. I,  $m_r$ ,  $m_b$  and  $m_h$  are the masses of the three links of a PCW module (a PCW is modelled as a 3 DOF serial manipulator) while the lengths of the links are  $r$ ,  $b$  and  $h$  respectively.

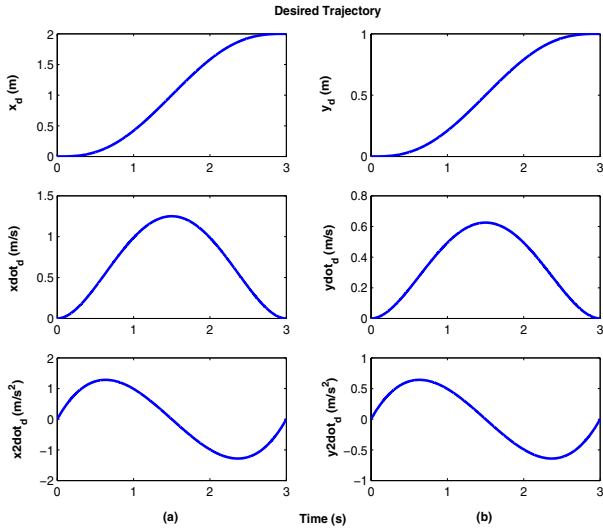


Fig. 5. Desired Trajectory

The desired trajectory used in the simulation is shown in Fig. 5. The robot was commanded to move 2 meters in  $x$  direction and 1 meter in  $y$  direction while maintaining the orientation of the robot. High order polynomials are used in the trajectory planning such that position, velocity and acceleration are all smooth. The non-slip condition for motion Eq. (14) is satisfied by choosing long enough duration of the trajectory.

### A. Effects of Wheel-Ground Interaction

In real situations, motion resistance generated by the wheel-ground interaction always exists, so the actual governing dynamic equations of motion of the robot are given by Eq. (10) rather than Eq. (7). In the case of trajectory tracking, control algorithms that consider wheel-ground interaction (e.g. Eq. (10)) are expected to demonstrate better tracking performance than those that do not consider the wheel-ground interaction (e.g. Eq. (7)).

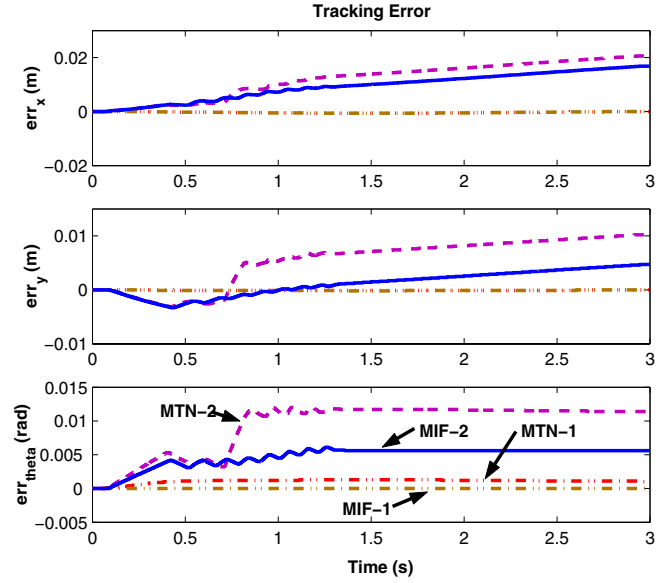


Fig. 6. Tracking errors. MTN-1/2: MTN scheme with/without considering wheel ground interaction; MIF-1/2: MIFDC scheme with/without considering wheel ground interaction

Fig. 6 shows the position and orientation tracking errors of different control schemes which are denoted by MTN-1, MTN-2, MIF-1 and MIF-2 respectively. MTN-1 (2) denotes MTN scheme with (without) considering wheel-ground interaction while MIF-1 (2) denotes MIFDC scheme with (without) considering wheel-ground interaction.

It can be observed from Fig. 6 that the tracking errors of MTN-1 and MIF-1 are much less than that of MTN-2 and MIF-2. This result shows that both position and orientation tracking errors can be reduced substantially when the wheel-ground interaction is considered in both torque distribution schemes. Also note that the tracking errors are comparable for MTN and MIFDC schemes.

### B. Effects of Torque Distribution

The actuation redundancy of the robot enables us to redistribute the joint torques such that non-slip conditions and actuator torque limit constraints are satisfied. Due to the utilization of different generalized inverse, the torque redistribution performances of the two proposed schemes are expected to be different.

We define the overall torque limits as  $T_{lim}$  based on the non-slip condition and actuator torque limits. In the case when particular joints violate the overall torque limits, null space joint torque vector  $\Gamma_o$  is computed such that those particular joint torques are regulated to be less than the torque limits  $T_{lim}$  e.g.  $p\%$  ( $0 < p < 100$ ) of  $T_{lim}$ .

Fig. 7 and Fig. 8 show the joint torques using scheme MTN and MIFDC respectively. Subfigure (a) and (b) in both figures are cases that are with/without torque limit constraints. Subfigure (a) in both figures are similar because no null space joint torque is generated and the difference is caused mainly

by the weighting effects of matrix  $\mathbf{B}$  which is relatively trivial.

However, in case when null space joint torque is generated (due to torque limit violation), the torque distribution capabilities of the two schemes are quite different which is shown in subfigure (b) of Fig. 7 and Fig. 8. Although those violated joints are regulated to be within the torque limit in both schemes, chattering is observed in case of scheme MTN (Fig. 7 (b)) while all the joints are within the torque limit in case of scheme MIFDC (Fig. 8 (b)). This example shows that scheme MIFDC has better performance in term of torque distribution than scheme MTN.

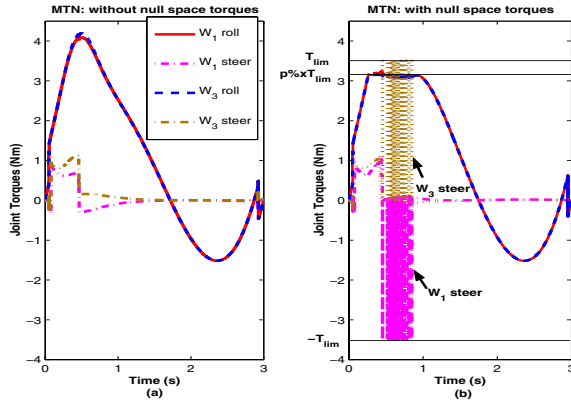


Fig. 7. Joint torques of MTN scheme. (a) without null space joint torques; (b) with null space joint torques

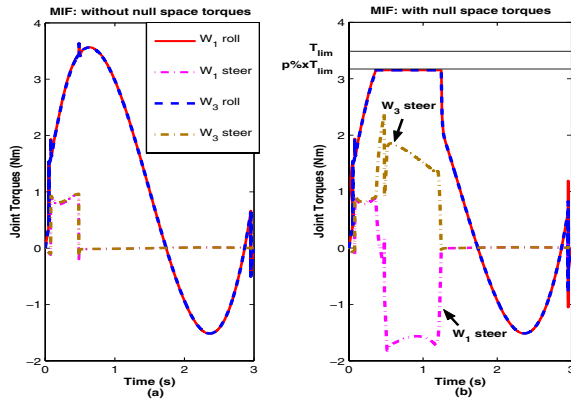


Fig. 8. Joint torques of MIF scheme. (a) without null space joint torques; (b) with null space joint torques

## VI. CONCLUSIONS

Based on vehicle dynamics analysis, wheel-ground interaction is modelled and compensated in the operational space dynamic model. Analytical conditions to avoid slipping are derived for both motion and torque. New torque distribution schemes are proposed to optimize specific criteria. Future work is to implement the proposed torque distribution schemes on the real robot. Another interesting extension would be to detect the actual slip of the wheels and utilize it to implement traction control on the mobile robot.

## ACKNOWLEDGMENT

The authors would like to thank Mr. Lim Chee Wang, Mr. Lim Tao Ming and Dr. Lim Ser Yong for their advices and discussions. The support of a collaborative research project grant from National University of Singapore and Singapore Institute of Manufacturing Technology (SIMTech) is gratefully acknowledged.

## REFERENCES

- [1] M. Zaw, D. Oetomo, Marcelo. H. Ang Jr., and T. Ng, "Kinematics and dynamics of an omnidirectional mobile platform with powered caster wheels," *Intl. Symp. Dynamics and Control*, 2003.
- [2] G. Campion, G. Bastin, and B. D'Andrea-novel, "Structural properties and classification of kinematic and dynamic models of wheeled mobile robots," *IEEE Trans. Robot. Automat.*, vol. 12, no. 1, pp. 47–62, February 1996.
- [3] R. Holmberg and O. Khatib, "Development and control of a holonomic mobile robot for mobile manipulation tasks," *Intl. J. Robotics Research*, vol. 19, no. 11, pp. 1066–1074, 2000.
- [4] B. Yi and W. Kim, "The kinematics for redundantly actuated omnidirectional mobile robots," *J. Robotic Systems*, vol. 12, no. 6, pp. 255–267, 2002.
- [5] J. H. Chung, B. Yi, W. Kim, and H. Lee, "The dynamic modeling and analysis for an omnidirectional mobile robot with three caster wheels," *Proc. IEEE Intl. Conf. Robotics and Automation*, vol. 1, pp. 521–527, 2003.
- [6] J. Park and C. Kim, "Wheel slip control in traction control system for vehicle stability," *Vehicle System dynamics*, vol. 31, pp. 263–278, 1999.
- [7] Y. Li, D. Oetomo, Marcelo. H. Ang Jr., and C. Lim, "Torque distribution and slip minimization in an omnidirectional mobile base," *Intl. Conf. Advanced Robotics*, pp. 567–572, 2005.
- [8] M. Bekker, *Theory of Land Locomotion*. University of Michigan Press, 1956.
- [9] J. Wong, *Theory of Ground Vehicles*, 3rd ed. John Wiley and Sons, Inc., 2001.
- [10] R. Holmberg and O. Khatib, "Development and control of a holonomic mobile robot for mobile manipulation tasks," *Intl. J. Robotics Research*, vol. 19, no. 11, pp. 1066–1074, 2000.
- [11] D. Oetomo, Y. Li, Marcelo. H. Ang Jr., and C. Lim, "Omnidirectional mobile robots with powered caster wheels: Design guidelines from kinematic isotropy analysis," *Proc. IEEE/RSJ Intl. Conf. Intelligent Robots and Systems*, pp. 2708–2713, 2005.
- [12] O. Khatib, "A unified approach for motion and force control of robot manipulators: The operational space formulation," *IEEE J. Robot. Automat.*, vol. RA-3, no. 1, pp. 43–53, 1987.
- [13] K. Chang, R. Holmberg, and O. Khatib, "The augmented object model: Cooperative manipulation and parallel mechanism dynamics," *Proc. IEEE Intl. Conf. Robotics and Automation*, vol. 1, pp. 470–475, 2000.
- [14] M. Smieszek, "Motion and energy consumption of automatically controlled transport vehicle - mobile robot," *Rzeszow Publishing House*, 2000.
- [15] Y. Nakamura, *Advanced Robotics: Redundancy and Optimization*. Addison-Wesley Publishing Company, 1991.
- [16] O. Khatib, "Motion/force redundancy of manipulators," *Japan-U.S.A. Symposium on Flexible Automation*, pp. 337–342, 1990.